Petroleum Science 22 (2025) 2604–2618

Contents lists available at ScienceDirect

Petroleum Science

journal homepage: www.keaipublishing.com/en/journals/petroleum-science

Original Paper

Effects of gas components on acid-rock reaction during CO_2-contained industrial waste gas (CO_2-contained IWG) injection into deep shale reservoir on geologic time scale

Yi-Fan Wang [a, b], Jing Wang [a, b, *], Hui-Qing Liu [a, b], Xiao-Cong Lv [a, b], Ze-Min Ji [c]

[a] National Key Laboratory of Petroleum Resources and Engineering, China University of Petroleum (Beijing), Beijing, 102249, China
[b] MOE Key Laboratory of Petroleum Engineering, China University of Petroleum (Beijing), Beijing, 102249, China
[c] Research Institute of Exploration and Development, PetroChina, Beijing, 100083, China

ARTICLE INFO

Article history:
Received 10 July 2024
Received in revised form
28 October 2024
Accepted 26 February 2025
Available online 27 February 2025

Edited by Min Li

Keywords:
CO_2-contained industrial waste gas
Geological sequestration
Shale
Kinetics model
Acid-rock reaction

ABSTRACT

The shortage of CO_2 source and the challenges associated with the separation of pure CO_2 have led to a growing interest in the potential utilization of CO_2-contained IWG. Therefore, this study has established an acid-rock interaction kinetic model to characterize the long-term interactions between CO_2-contained IWG and shale. The findings delineate the reaction process into three phases: during the initial 10 years, solubility trapping predominates, with minimal mineral dissolution. This increases shale porosity, promoting the diffusion and storage range of CO_2-contained IWG. Between 10 and 300 years, mineral dissolution/precipitation assumes primacy, with mineral trapping gradually supplanting dissolution. Notably, shale porosity diminishes by a minimum of approximately 40%, effectively inhibiting gas leakage. After 300 years, equilibrium is reached, with rock porosity consistently lower than the initial porosity. Throughout the entire reaction process, as the initial CO_2 concentration decreases, the initial pH drops from 4.42 to 3.61, resulting in a roughly 20% increase in porosity. Additionally, it is necessary to regulate its concentration to avoid H_2S leakage during CO_2-contained IWG geological sequestration. And particular attention should be directed towards the risk of gas leakage when the IWG exhibit high levels of SO_2 or NO_2.

1. Introduction

The significant population growth and excessive dependence of humanity on fossil fuels since the Industrial Revolution have led to the substantial emission of greenhouse gases, primarily CO_2, resulting in air pollution and global climate change (Zou et al., 2023; Fatah et al., 2024). At present, CO_2 emissions reduction has become a focal point of global concern, and carbon capture, utilization, and storage (CCUS) is considered the most promising technology to achieve CO_2 reduction goals in the next 10–20 years (De Silva et al., 2015; Teng et al., 2019; Fatah et al., 2020; Song et al., 2023). Nevertheless, excessive cost of CO_2 capture and the considerable challenges associated with the separation of pure CO_2 have resulted in a limited availability of CO_2 gas sources for geological sequestration (Yin et al., 2016; Zou et al., 2023). Besides, industrial emissions from sources such as power plants and chemical factories, which contain impurity gases like CO, SO_2, NO_2, H_2S, and HF, constitute the largest contributors to CO_2 emissions (Li et al., 2010; Ghayur et al., 2019; Zhang et al., 2022). If these CO_2-contained IWG can be injected directly into subsurface formations, allowing them to dissolve or react fully within the formations, there would be no need for pre-treatment of IWG during the carbon capture stage. This approach could significantly reduce the cost of industrial gas treatment (Chialvo et al., 2013), increase the feasibility of commercial-scale CCUS implementation, and undoubtedly accelerate the achievement of carbon emissions reduction and carbon neutrality objectives.

Shale formations, due to their extensive distribution and excellent adsorption properties, hold significant potential for CO_2 geological sequestration (Kang et al., 2011; Middleton et al., 2015; Liu et al., 2016; Zhan et al., 2017; Fatah et al., 2020). Existing research indicates that CO_2-contained IWG, which includes CO_2,

* Corresponding author.
E-mail address: wangj@cup.edu.cn (J. Wang).

https://doi.org/10.1016/j.petsci.2025.02.023

CO, SO_2, NO_x, H_2S, HF, etc., exhibit strong adsorption capabilities on the surface of shale, surpassing that of CH_4 (Merey and Sinayuc, 2016; Huang et al., 2019; Wang et al., 2022). During the geological sequestration of CO_2-contained IWG into shale gas reservoir, the extraction and dissolution effects of acidic gases on shale can increase the porosity and permeability, effectively enhancing shale gas production (Godec et al., 2013; Zhan et al., 2017; Lyu et al., 2018; Zhou et al., 2019). Additionally, this process can expand the diffusion range and sequestration capacity of CO_2-contained IWG within shale gas reservoir, thereby enhancing the long-term stabilization of CO_2-contained IWG sequestration (Ao et al., 2017; Song et al., 2019). Nevertheless, injecting CO_2-contained IWG into shale gas reservoir can lead to chemical reactions with minerals, resulting in changes in pore structure, mechanical properties, surface characteristics, and other physical properties of shale (Rezaee et al., 2017; Fatah et al., 2021). Current research has not fully comprehended the interaction of CO_2-contained IWG with shale minerals. The outcomes of these acid-rock interactions could be advantageous for CO_2-contained IWG geological sequestration, but they may also increase the risk for the leakage of CO_2-contained IWG (Liu et al., 2016). Consequently, comprehensive investigation into the interaction processes involving CO_2-contained IWG, shale minerals, and water is imperative, along with the assessment of their impact on the prolonged CO_2-contained IWG sequestration stabilization in shale reservoir.

Currently, several laboratory experiments and numerical simulation studies have been conducted to evaluate the occurrence of acid-rock reactions during CO_2 and IWG geological sequestration processes, as well as their impact on reservoir properties (Crandell et al., 2010; Yin et al., 2016; Rezaee et al., 2017; Hadian and Rezaee, 2019; Hui et al., 2019; Wang et al., 2019; Fatah et al., 2022). The research findings indicate that the interactions between CO_2, water, and rocks ultimately lead to a reduction in cap rock porosity, which is favorable for the long-term geological sequestration of gases. This is attributed to the fact that during extended CO_2 geological sequestration, calcite and clay minerals undergo dissolution reactions in acidic aqueous solutions, resulting in the precipitation of minerals such as quartz, calcite, dawsonite, and kaolinite (Bhuiyan et al., 2020). This reduces the diffusion range of CO_2, mitigates the risk of CO_2 leakage, thereby strengthening the stabilization of geological sequestration (Tian et al., 2014; Bhuiyan et al., 2020). However, the injection of IWG such as SO_2, NO_2, and H_2S into shale can lead to hydrolysis reactions or redox reactions, generating acidic solutions such as sulfurous acid, sulfuric acid, and nitric acid. These strong acids significantly reduce the pH of formation water, accelerate mineral dissolution and precipitation, thereby altering shale porosity and permeability, affecting the integrity of reservoir rocks and caprocks, and posing a threat to CO_2-contained IWG sequestration stability (Rochelle et al., 2004; Gaus et al., 2005; Kutchko et al., 2007; Ellis et al., 2010; Pan et al., 2018). However, existing research mostly focuses on the impact of pure CO_2 or single IWG on conventional reservoir geological sequestration, lacking the impact of CO_2-contained IWG-water-shale minerals interaction on long-term stability of geological sequestration.

This paper aims to characterize the kinetic reactions of CO_2-contained IWG-water-shale and provide geological timescale results of these reactions by establishing a core-scale water-rock reaction kinetic model. It delineates the variations in the pH of the solution, gas dissolution, shale mineral dissolution/precipitation, and rock porosity during water-rock reactions under different CO_2 concentrations and predominant gas conditions. These findings contribute to a deeper understanding of the characteristics of CO_2-contained IWG-brine-shale reactions and provide a basis for assessing the prolonged CO_2-contained IWG sequestration stabilization in shale reservoir.

2. Numerical modeling approach

2.1. Theoretical approach

Currently, the physical parameters of reservoir during geologic sequestration are mainly studied by water-rock reaction kinetics. Thus, in this paper, the 1D core-scale kinetic model was established to characterize CO_2-contained IWG-water-shale interactions. In this model, the equilibrium process between CO_2-contained IWG and aqueous solution is thermodynamically controlled, while the dissolving and precipitating processes of shale within the aqueous solution are kinetically controlled. The theories and equations used in this model have been extensively validated and are highly reliable in accurately and efficiently simulating acid rock reactions during geologic sequestration. In addition, since most of the existing studies have focused on the interaction of pure CO_2 with minerals and there are synergistic as well as antagonistic interactions between the various gases, the reaction database of the present model has been rewritten to accurately simulate the interactions between CO_2-contained IWG, brine and shale.

In a shale mineral kinetic reaction, the concentration of substances in brine are described as (Zhu and Anderson, 2002):

$$\frac{\mathrm{d}m_i}{\mathrm{d}t} = c_{i,\mathrm{k}} R_{\mathrm{k}} \tag{1}$$

where, $c_{i,\mathrm{k}}$ represents stoichiometric coefficient of substance i within the dissolution/precipitation reaction of mineral k; R_{k} represents dissolution/precipitation reaction rate of mineral k, mol/(kg·s). Generally, the dissolution/precipitation rate varies depending on the progression of the reaction, necessitating the solution of a set of ordinary differential equations.

Through water-rock interaction experiments, extensive kinetic rates under various temperature, pressure, and aqueous solution composition conditions have been measured. Nevertheless, various scholars employ differing rate formulations to match the actual reaction. In this model, a simplified kinetic reaction equation is used, where the total kinetic reaction rate of shale minerals is represented as (Palandri and Kharaka, 2004):

$$R_{\mathrm{k}} = r_{\mathrm{k}} \frac{A_0}{V} \left(\frac{m_{\mathrm{k}}}{m_{0\mathrm{k}}} \right)^n \tag{2}$$

where, r_{k} represents specific rate of kinetic reaction of mineral k, mol/(m^2·s); V represents the mass of brine, kg; A_0 represents the reactive surface area of mineral at initial state, m^2; m_{k} represents the molarity of the mineral at that moment; $m_{0\mathrm{k}}$ represents the initial molarity of the mineral; $(m_{\mathrm{k}}/m_{0\mathrm{k}})^n$ represents a parameter that accounts for the selective dissolution and aging of the mineral, as well as changes in A_0/V during the mineral dissolution/precipitation process. homogeneously dissolved sphere and cube, n is typically set to 2/3. Various expressions exist for the specific rate r_{k} of shale mineral kinetic reactions, and their form largely depends on the comprehensiveness of information from physical simulation experiments. Currently, the following general formula is commonly used in kinetic simulations of water-rock reactions (Steefel and Lasaga, 1994):

$$r_{\mathrm{k}} = k_{\mathrm{k}} \left[1 - \left(\frac{\mathrm{IAP}}{K_{\mathrm{k}}} \right)^{\sigma} \right] \tag{3}$$

where, k_{k} represents the temperature-dependent rate constant, mol/(m^2·s); K_{k} represents the equilibrium constant for mineral

dissolution/precipitation reaction; IAP represents the ion activity product; the correction factor σ typically set to 1. In this rate equation, IAP/K_k indicates the saturation ratio for dissolution/precipitation of mineral k, with dissolving reaction occurring at IAP/$K_k > 1$ while mineral precipitation occurring at IAP/$K_k < 1$. The merit in the rate formulation is that it works for both oversaturated as well as undersaturated states and becomes zero at equilibrium. When the mineral dissolution/precipitation reaction is far from equilibrium, the rate remains constant over a wide range (IAP/$K_k < 0.1$), while the rate is close to zero as the reaction nears equilibrium (IAP/K_k approaches 1).

The rate constant k_k for shale mineral kinetic reactions is calculated using the following formula (Lasaga, 1984):

$$k_k = k_{25} \exp\left[-\frac{E_a}{R}\left(\frac{1}{T} - \frac{1}{298.15}\right)\right] \tag{4}$$

where, k_{25} represents the rate constant at 298.15 K, mol/(m^2·s); E_a represents the activation energy, J/mol; T is the simulation temperature, K; R is the gas constant which takes the value of 8.314 J/(mol K). In this model, activation energy rate constant at 298.15 K for mineral-brine-rock reactions are obtained from the literature (Gherardi et al., 2007), as shown in Table 1. This data is widely used in all types of acid-rock response simulations and has a high degree of accuracy.

In kinetic simulations of water-rock reactions, the equilibrium constant K_k plays a crucial role in calculating gas solubility and the dissolving and precipitation processes of shale minerals in geological sequestration of CO_2-contained IWG. K_k as a parameter related to temperature which could be represented by the following equation:

$$\lg K_k = A_1 + A_2 T + \frac{A_3}{T} + A_4 \lg T + \frac{A_5}{T^2} + A_6 T^2 \tag{5}$$

where, A_1–A_6 are constant which sourced from LLNL database. In reaction kinetic calculation among CO_2-contained IWG, water, and mineral, reactive surface area for each mineral involved in the reaction is crucial, as it significantly influences the result in acid-rock interaction. In this paper, it is assumed that minerals consist of ideal spherical particles (Koukouzas et al., 2018), with the particle diameter of non-clay mineral (calcite, quartz, albite, dolomite, K-feldspar, dawsonite, pyrite) being 3.3×10^{-5} m, while the particle diameter of clay minerals (illite, montmorillonite, kaolinite) is 2×10^{-6} m (Mohd Amin et al., 2014). Then, according to the molar mass and molar volume of each mineral, the mineral surface area required for the water-rock reaction kinetics is calculated. This method, compared to the BET method, can more accurately calculate the mineral reaction surface area for core-scale water-rock reactions and the influence of irregular mineral shapes on the dissolution and precipitation rates of minerals is limited (Xu et al., 2010; Van Pham et al., 2012; Koukouzas et al., 2018; Hadian and Rezaee, 2019). The specific calculation formula is as follows:

$$\rho = \frac{V_m}{M} \tag{6}$$

$$V_s = \frac{3}{4}\pi r^3 \tag{7}$$

$$A_s = 4\pi r^2 \tag{8}$$

$$A = \rho \frac{A_s}{V_s} \tag{9}$$

where, V_m represents molar volume for each shale mineral, m^3/mol; M represents molar mass for each shale mineral, g/mol; V_s represents volume for mineral sphere, m^3; ρ represents density for each shale mineral, g/m^3; A_s represents surface area for mineral sphere, m^2; r represents radius for mineral sphere, m; A represents reactive surface area for each shale mineral, m^2.

The equations obtained from the above expressions provide the kinetic rate equations for various minerals involved in interaction between CO_2-contained IWG, water, and shale minerals. Since reaction rates vary with time, it is necessary to integrate them over the specified simulation time. This includes calculating the concentrations for each species in brine and simultaneously calculating the changes in reaction rates. In this paper, the reaction kinetic model for CO_2-contained IWG-water-shale is solved using Runge-Kutta (RK) method. This algorithm integrates the time-varying reaction rates and ultimately provides the status for whole chemical system at a given simulation time.

After calculating the amount of each mineral in the shale during the geological sequestration process, the shale porosity can be calculated by the change in mineral volume during the reaction process, which is shown in the following formula:

$$\phi = 1 - \sum_{k}^{N_k} \frac{V_k}{V_{rock}} \tag{10}$$

where, ϕ is the rock porosity; N_k is the number of minerals in the rock; V_k is the volume of mineral k in the rock, m^3; V_{rock} is the total rock volume, m^3.

2.2. Model concepts

In this paper, the 1D core scaled water-rock reaction kinetic model (see Fig. 1) is established in order to emulate the interaction between CO_2-contained IWG, brine, and shale minerals under CO_2-contained IWG shale reservoir sequestration. Shale mineral composition of the core sample used for kinetic model is

Table 1
Kinetic parameters of shale minerals in this model (Gherardi et al., 2007).

Mineral	Mole mass, g/mol	k_{25}, mol/(m^2·s)	E_a, kJ/mol	Specific surface area, m^2/g
Quartz	60	1×10^{-14}	87.7	0.0686
Calcite	100	1.6×10^{-6}	23.5	0.0671
Dolomite	184	3×10^{-13}	52.2	0.0638
Albite	262	2.8×10^{-13}	69.8	0.0693
K-feldspar	278	3.9×10^{-13}	38	0.0702
Illite	383.5	1.7×10^{-13}	35	1.0909
Montmor-Ca	365.61	1.66×10^{-13}	35	1.2
Pyrite	120	4×10^{-11}	62.76	0.0371
Kaolinite	258	6.9×10^{-14}	22.2	1.1538
Dawsonite	144	1.3×10^{-9}	62.8	0.0748

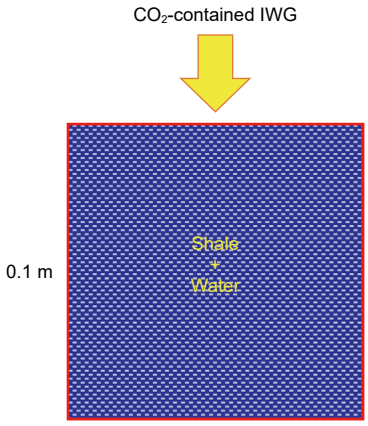

Fig. 1. Schematic diagram of the 1D core-scale water-rock reaction kinetics model.

summarized by Table 2. The mineralogical composition is referenced from the deep Longmaxi shale in southern Sichuan Basin, which pore and fracture types are mainly nanometer-sized pores and tectonic fractures, with abundant contents of quartz as well as clay mineral, each constituting over 30% of the composition. The sample also contains minor amounts of feldspar (albite and K-feldspar), carbonate minerals (calcite and dolomite), and pyrite. Besides, according to the literature, it is known that the reservoir temperature is 100–120 °C and reservoir pressure is 70–120 MPa for deep Longmaxi shale in southern Sichuan Basin, so the pressure and temperature of the kinetic model are set to 70 MPa and 110 °C. The kinetic model was conducted under isothermal conditions at 110 °C, assuming a 0.1 × 0.1 × 0.1 m cubic rock with an initial porosity of 10% and pure water filling the rock pores. Therefore, the total porous medium volume in this model is 1×10^{-3} m^3, which contains 0.1 kg of water. CO_2-contained IWG (gas composition as CO_2, NO_2, CO, SO_2, H_2S, HF) was used to fill the rock pore space at a pressure of 70 MPa (constant volume of 1×10^{-4} m^3), simulating the interaction between CO_2-contained IWG, brine, and mineral of shale for 1000 years. Since this model operates at the core scale, no-flow boundaries were set as the boundaries of the model.

2.3. Model validation

Since the estimated values of mineral surface area can often differ from actual values, to ensure the precision in simulated results for the CO_2-contained IWG-brine-shale chemical kinetic model, we compared and validated the model against experimental results conducted by literature (Fatah et al., 2021). Existing experimental research data are mainly based on the CO_2-brine-shale reaction, and relatively little experimental data are currently available for the CO_2-contained IWG-brine-shale reaction. Since the composition of CO_2-contained IWG in this study is dominated by CO_2, this study simulates the chemical reaction between CO_2 and Mancos shale to verify the accuracy of CO_2-contained IWG-brine-shale reaction model. This literature has examined the water-rock reaction of sc-CO_2 with Mancos shale mineral powder under temperature conditions of 70 °C and pressure conditions of 177 atm. The composition of the shale minerals used in their experiment is similar to the shale sample used in this paper. The reaction time in their experiment was 30 days. Therefore, using under the same simulated conditions (mineral fraction, brine fraction, temperature, pressure, simulation time) in this kinetic model to compare the mass fractions of minerals in the reacted shale, and the comparison results are presented as Fig. 2. From comparative validation results, it is evident that after water-rock reaction, the shale's quartz content increases, while the content of carbonate minerals and clay minerals decreases. This matches the experimental results, and the comparison between the simulation results and experimental data shows a relatively small discrepancy (with errors ranging from 2% to 6%). The source of the error might be the estimation of mineral reaction surface area in this model using the geometric calculation method, which tends to underestimate the mineral's surface area (Koukouzas et al., 2018). This could result in a slightly lower quartz content and slightly higher content of minerals like illite, calcite, K-feldspar, and kaolinite compared to the experimental results. In summary, we believe that this kinetic model could be used to precisely emulate the interactions between CO_2-contained IWG, brine, and shale minerals.

3. Results and discussion

3.1. Water-rock reaction results under different CO_2 concentrations

The established chemical reaction kinetic model was employed to emulate the interactions of CO_2-contained IWG, brine, and shale

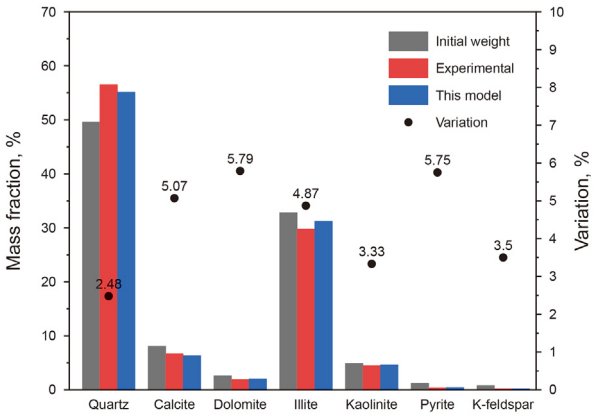

Fig. 2. Validation of this model with experimental data (Fatah et al., 2021).

Table 2
Mineral contents of shale samples.

Mineral	Chemical formula	Molecular weight, g/mol	Mass fraction, %	Amount, mol
Quartz	SiO_2	60	38.7	15.7722
Calcite	$CaCO_3$	100	6.4	1.565
Dolomite	$CaMg(CO_3)_2$	184	4.7	1.1562
Albite	$NaAlSi_3O_8$	262	4.1	0.3827
K-feldspar	$KAlSi_3O_8$	278	3.3	0.2815
Illite	$K_{0.6}Mg_{0.25}Al_{2.3}Si_{3.5}O_{10}(OH)_2$	383.5	25.4	1.6196
Montmor-Ca	$Ca_{0.165}Mg_{0.33}Al_{1.67}Si_4O_{10}(OH)_2$	365.6	10.2	0.6822
Pyrite	FeS_2	120	3.2	0.6725
Kaolinite	$Al_2Si_2O_5(OH)_4$	258	0	0
Dawsonite	$NaAlCO_3(OH)_2$	144	0	0

over a period of 1000 years at different CO_2 concentrations. The initial fugacity of pure CO_2 (in this study, fugacity is assumed to be the partial pressure in the gas phase) was set at 70 MPa. As the concentration of IWG increases, the initial fugacity of CO_2 gradually decreases until zero. The model provided the changes in solution pH, gas solubility, shale mineral dissolution/precipitation, porosity, and sequestration capacity due to dissolution and mineralization throughout the CO_2-contained IWG-brine-shale reaction process.

3.1.1. Changes in pH of aqueous solutions

The changes of solution pH during the CO_2-contained IWG-brine-shale reaction at different CO_2 concentrations were illustrated as Fig. 3. According to the results, after injecting pure CO_2 into the water-shale system for 0.1 year, the pH decreases from 7.0 to below 4.5 and gradually increases to 5.19 over the course of 1000 years. Furthermore, as the initial concentrations of CO_2 within the CO_2-contained IWG decreases, the pH of aqueous solution gradually decreases. It is due to the increase in the initial concentration of SO_2 in the IWG, which readily dissolves in water and forms strong acids like H_2SO_3 (Zhu et al., 2019; Turner et al., 2022). This leads to an enhancement in H^+ concentration within aqueous solution. Importantly, these hydrogen ions are not entirely neutralized through reactions with shale minerals (mainly carbonate minerals), ultimately leads to reduction in pH of aqueous solution.

The CO_2 and IWG concentrations in CO_2-contained IWG influence the H^+ concentration that can react within aqueous solution, subsequently affecting the aqueous solution pH for the acid-shale interaction process (Pearce et al., 2016; Liu et al., 2019). The H^+ within water solution are continuously consumed through the dissolving and precipitation reactions for shale mineral within water, resulting in a gradual increase of aqueous solution pH in the later stages of water-rock reactions. After 300 years of reaction, the pH of the solution no longer shows significant changes. This is because at this point, the gas has dissolved and precipitated in the minerals to near saturation, and the interaction of CO_2-contained IWG, brine, and shale minerals reaches equilibrium.

3.1.2. Changes in gas components in the gas phase

The changes of gas components during the CO_2-contained IWG-brine-shale reaction at various CO_2 concentrations were illustrated as Fig. 4. It can be observed that after injecting CO_2-contained IWG into the shale reservoir for 0.1 year, NO_2, HF, SO_2, CO within the gas phase is completely consumed, while CO_2 and H_2S are partially consumed. This is because NO_2, SO_2, HF have strong solubility within brine and thus dissolve completely in the aqueous phase (Turner et al., 2022). CO_2 and H_2S have weaker solubility in water, so they only partially dissolve. Although CO is poorly soluble within brine, it could be oxidized to generate CO_2, ultimately resulting in complete consumption of CO in the gas phase. Differences in solubility between gases affect their distribution in the reservoir and their reactions with minerals. Gases with higher solubility (e.g., NO_2, SO_2) are mainly distributed in formation water in the reservoir, diffusing and triggering extensive mineral dissolution, whereas gases with lower solubility (e.g., H_2S, CO_2) are usually present in gaseous state and are concentrated in a specific area, which may have localized impact on mineral dissolution in the reservoir. With the reduction in the initial CO_2 concentration of CO_2-contained IWG, the amount for CO_2 in the gas phase gradually decreases in the early stages for acid-rock reaction then reaches equilibrium. The amount for H_2S in the gas phase increases gradually in the early stages of the reaction and reaches equilibrium. When the concentration of IWG within CO_2-contained IWG is excessively large, the high H^+ concentrations within brine causes them to react extensively with carbonate minerals (primarily calcite), leading to the generation of a small amount of CO_2. In addition to the conversion of CO, this causes the amount of CO_2 for gas phase being higher than its initial value at the beginning of the water-rock reactions.

As the interaction between CO_2-contained IWG with brine and minerals continues over 1000 years, the gases in the gas phase exhibit consistent behavior. NO_2, HF, SO_2, CO were totally exhausted in gas phase throughout the reaction. The amount of H_2S in the gas phase is mostly consumed at the beginning for the interaction and remains almost constant. The amount for CO_2 in the gas phase is partially exhausted at the beginning for the interaction, gradually decreases within 100 years for water-rock reaction, sharply declines between 100 and 300 years, and eventually levels off after 300 years of water-rock reaction. This is due to dissolving and precipitation for shale mineral within the aqueous solution, leading to the consumption of H^+ in brine. The dissolving and precipitation reactions for the shale mineral primarily occur between 100 and 300 years of water-rock reaction. During this period, H^+ concentrations of brine drop sharply, and the precipitation of carbonate minerals consumes a significant amount of carbonate ions in brine, leading to dissolution of a substantial portion of CO_2 in the gas phase into the water. Besides, the interaction between gases produces obvious synergistic and antagonistic effects. SO_2, NO_2 and other gases with strong solvency capacity will release a large number of H^+ when dissolved in brine, thus inhibiting the dissolution of CO_2, H_2S and other gases. Among them, a chemical reaction may occur between H_2S and SO_2 to generate S and water. This reaction can inhibit further reaction between SO_2 and reservoir minerals, thus reducing the acidification of SO_2 and slowing down mineral dissolution.

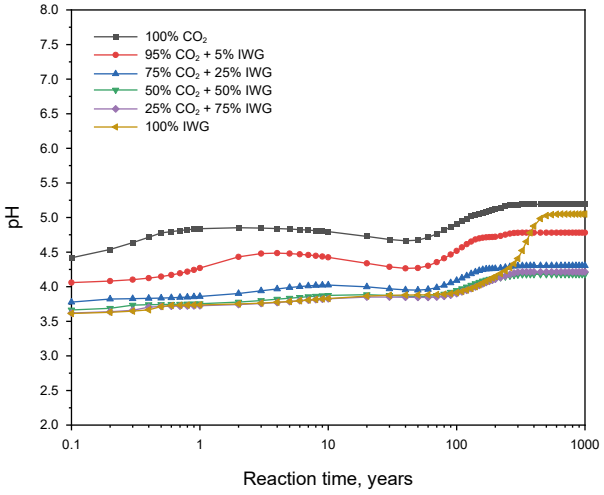

Fig. 3. Changes of pH during water-rock reaction with different CO_2 concentrations.

3.1.3. Changes in mineral dissolution/precipitation

The changes of shale minerals during the CO_2-contained IWG-brine-shale reaction under various CO_2 concentrations were illustrated as Fig. 5. From the results, it can be seen that upon reaching equilibrium in interaction of CO_2-contained IWG with brine and shale minerals, albite, illite, montmorillonite is completely dissolved, calcite partially dissolves, while pyrite is minimally involved in the reaction; the reaction also results in the sedimentation in quartz, K-feldspar, dolomite, dawsonite, kaolinite, of which dawsonite and kaolinite were secondary mineral. With a decrease in the initial concentrations for CO_2 from the CO_2-contained IWG, the dissolution of calcite increases at the beginning period for the interaction due to the heightened acidity for the aqueous solution.

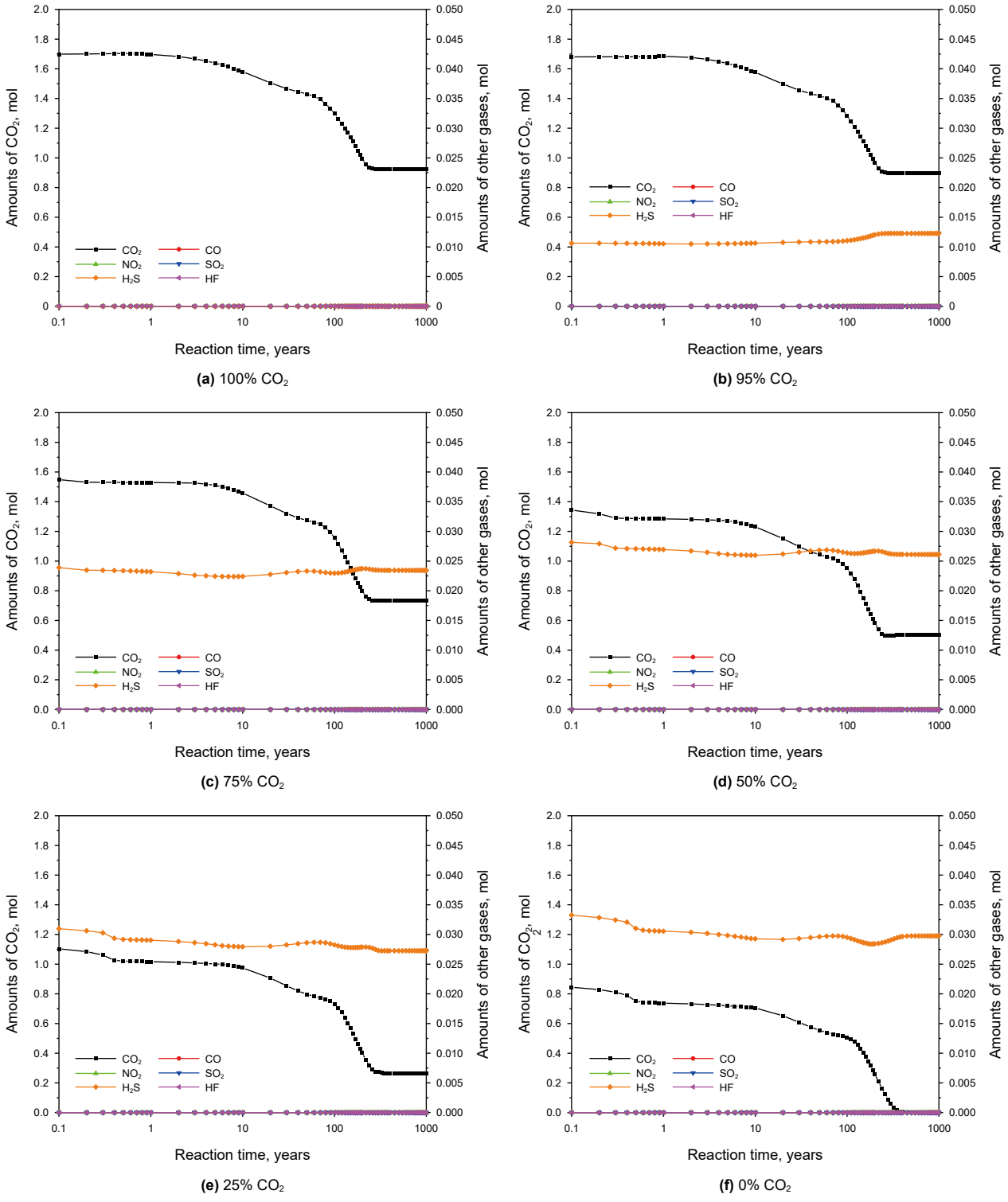

Fig. 4. Changes of gas components during water-rock reaction with different CO_2 concentrations.

However, at equilibrium, a reduced initial CO_2 concentration leads to increased calcite dissolution. Simultaneously, the precipitation for kaolinite, K-feldspar intensifies, while the precipitation for dolomite, quartz, dawsonite decreases. This is attributed to the increasing concentrations for IWG from the CO_2-contained IWG, resulting in a decrease in the pH for brine throughout the entire reaction period, thereby promoting the extent of mineral dissolution/precipitation reactions. Consequently, calcite dissolution and the precipitation of K-feldspar and kaolinite increase. Secondly, the diminished concentration of carbonate ions within brine, because of the reduced concentration of CO_2, resulting in decreased precipitation for dolomite and dawsonite. Finally, the increased dissolution reactions of calcite and intensified precipitation reactions of K-feldspar and kaolinite further lead to a

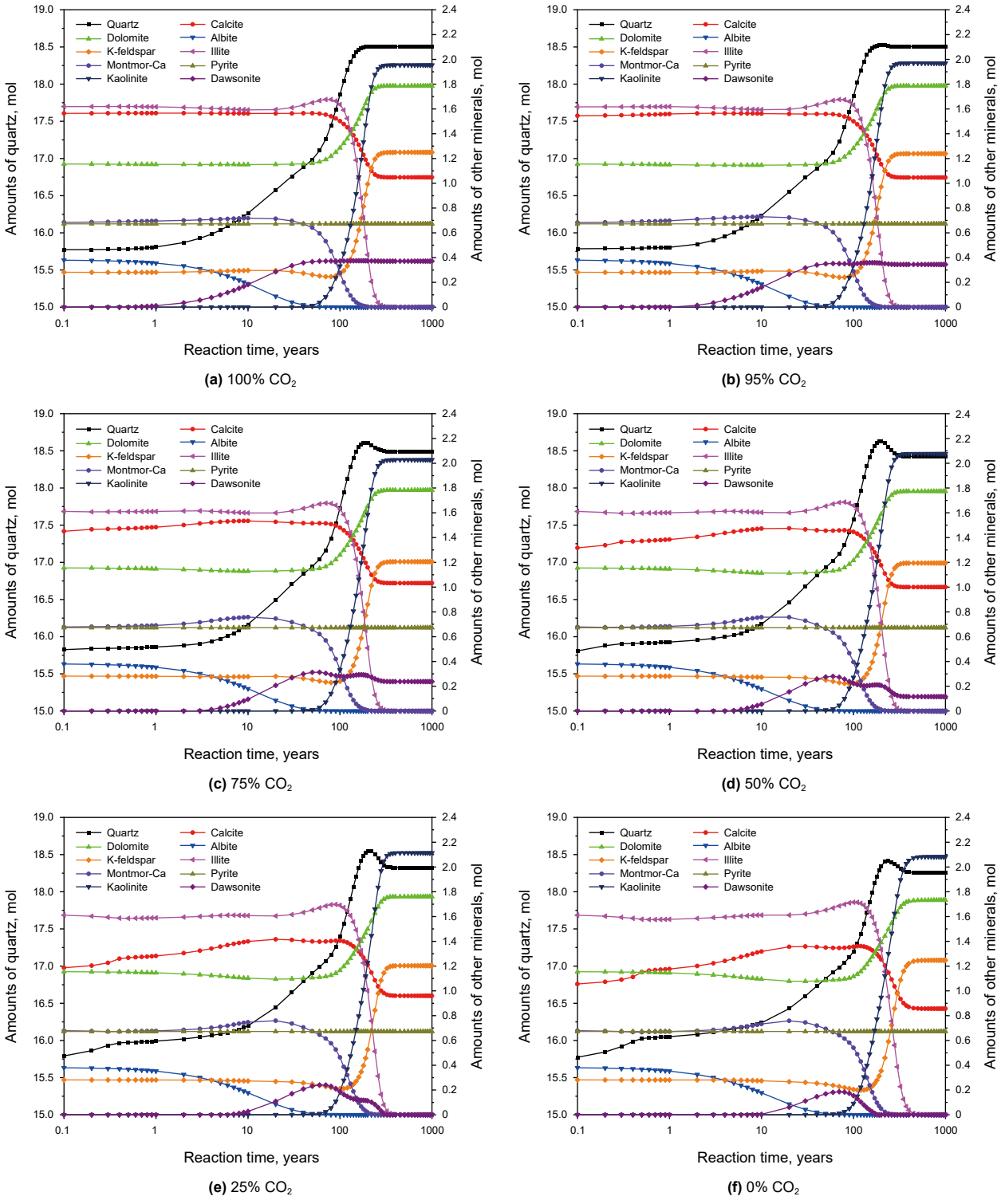

Fig. 5. Changes of shale minerals during water-rock reaction with different CO_2 concentrations.

reduction in quartz precipitation, as quartz primarily forms through the dissolution reactions of silicate minerals.

As interaction between CO_2-contained IWG with brine and shale minerals continues, it is evident that shale mineral has been dissolved or precipitated mainly occur between 10 and 200 years, reaching an equilibrium state after 300 years. In the initial 0.1 years of the reaction, only partial dissolution of calcite in shale minerals is observed. Over the period from 0.1 years to 100 years, the dissolution of calcite gradually increases, and it rapidly dissolves between 100 and 300 years until equilibrium is reached. Dolomite remains relatively constant in the first 50 years but subsequently precipitates until equilibrium is achieved. Albite, illite, and montmorillonite in the clay minerals exhibit behavior similar to calcite. Albite gradually increases in dissolution with time, dissolving

completely after 50 years. Illite and montmorillonite dissolved progressively more with time and reached equilibrium in 300 years, in which the findings were in agreement with those of related studies (Liu et al., 2016). The behavior for quartz, kaolinite, K-feldspar, dawsonite is similar. Their amounts remain relatively stable in the early stages of the reaction, with gradual increases in precipitation occurring in the mid-term until equilibrium is achieved. Dawsonite exhibits a unique behavior with initial precipitation followed by dissolution at lower initial CO_2 concentrations. This is due to the decreasing concentration of carbonate ions in the aqueous solution during the later stages of the reaction, coupled with the precipitation of dolomite, which promotes the dissolution reaction of dawsonite.

Based on the simulation results from Fig. 5, the dynamic process for CO_2-contained IWG-brine-shale interaction could be separated in three stages. Firstly, during initial decade for acid-rock reaction, the primary reactants are albite and calcite. These two minerals start dissolving slightly, generating small amounts of quartz, montmorillonite, and dawsonite precipitation. Subsequently, in the second phase, the shale mineral dissolving and precipitating reactions rapidly increase then continue for approximately 300 years. Finally, during the third stage (over 300 years later), minerals continue undergoing slight dissolution/precipitation until equilibrium is reached. The dissolution/precipitation behavior of calcite in this simulation aligns with existing finding (Hellevang et al., 2013), which suggests that the reaction for CO_2-contained IWG, water, and shale minerals in the first 10 years gradually leads to calcite dissolution, with subsequent dissolution increasing rapidly up to the point where equilibrium is reached around 300 years. There was no significant reaction of minerals including dolomite, pyrite, kaolinite, K-feldspar in the first stage. However, in the second phase, their dissolution/precipitation reactions intensified which continue up to the beginning in third stage when equilibrium is reached. According to existing literature (Zhu et al., 2019; Cheng et al., 2020), during early stages of the water-rock reaction, quartz experiences minimal dissolution. Nevertheless, with the progress in acid-rock reaction, dissolving process for montmorillonite and illite results in massive precipitation on quartz particles. Such interactions made quartz particles become more stabilized under acidic environment, which accelerated precipitation of quartz. Additionally, the simulated outcomes from Fig. 5 suggest that the content of shale minerals significantly changes during the second phase for interaction between CO_2-contained IWG, brine, and shale mineral. This makes mineral trapping became primary mechanism for CO_2 geological sequestration in shale formations. Currently, most of the existing studies focus on the water-rock reaction between pure CO_2 and rocks, and there are fewer studies on industrial waste gases, which have not evaluated the influence of impurity gases on the stability of geological sequestration during the geological sequestration process of CO_2-contained IWG. Therefore, the novelty of this study is to clarify the influence of CO_2-contained IWG with different gas components on the geological sequestration process. Compared with the pure CO_2-brine-rock reaction, the acid-rock reaction of CO_2-contained IWG with shale is more intense, and the dissolution and precipitation of minerals are more significant.

3.1.4. Changes in shale porosity

The changes of shale porosity during the CO_2-contained IWG-brine-shale reaction at various CO_2 concentrations were illustrated as Fig. 6. From the results, it can be seen that after injecting CO_2-contained IWG into the water-shale system for 0.1 year, the porosity increases. Subsequently, over a period of 1000 years, it gradually decreases until stabilizing, ultimately reaching a value lower than the initial porosity. This decrease in porosity is advantageous of the long-term stabilization for CO_2-contained IWG

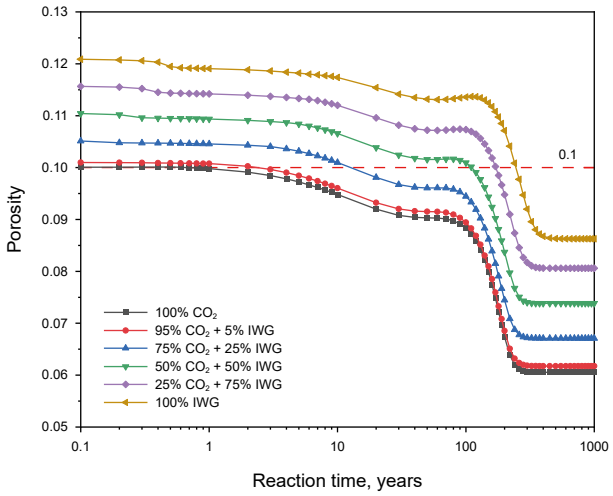

Fig. 6. Changes of shale porosity during water-rock reaction with different CO_2 concentrations.

geological sequestration in shale formations. As original concentrations for CO_2 from CO_2-contained IWG decreases, shale porosity gradually increases throughout the entire reaction period. This is due to the enhanced acidity of the aqueous solution, which promotes the dissolution of minerals and, consequently, leads to an increase in rock porosity.

As the water-rock reaction progresses, the rock porosity undergoes distinct changes over time. Initially, within the first 0.1 year of the reaction, the rock porosity increases. From 0.1 year to 100 years into the reaction, rock porosity experiences a gradual reduction. Then, in the 100-year to 300-year timeframe, there is a significant and rapid decrease in porosity. Eventually, after 300 years of the reaction, it stabilizes, and no further changes are observed. This evolution can be attributed to the various stages for interaction between CO_2-contained IWG, brine, and shale minerals. In early stages, the dominant reactions involve albite and calcite dissolution, resulting in the increasing for shale porosity. In mid-phase for CO_2-contained IWG-brine-shale interaction, as shale minerals precipitation reactions intensify, rock porosity gradually decreases. Between 100 and 300 years, significant precipitation reactions occur, causing a sharp reduction in rock porosity. Finally, as the CO_2-contained IWG-brine-shale interaction reaches equilibrium, shale porosity stabilizes. The patterns in shale porosity change provide valuable insights into the process of the CO_2-contained IWG injection in shale reservoir. In the initial phases, increased porosity allows gases to diffuse over a wider area, enhancing the storage capacity for CO_2-contained IWG. However, as the acid-rock reaction progresses, the gradual reduction in porosity limits gas migration, improving the long-term stability of geological sequestration. Over the entire process of CO_2-contained IWG geological storage, the significant reduction in shale porosity is advantageous for the stability of geological sequestration (Xu et al., 2019; Yang et al., 2020; Fatah et al., 2021). Besides, since the acid-rock reaction takes place on geological time scale, the reaction rate is relatively slow, resulting in a reduction in reservoir porosity that occurs slowly, and therefore there is no risk of excessive pressure buildup that could result in gas leakage.

3.1.5. Changes in dissolved and mineralized sequestration

The changes of sequestration capacity and rate due to dissolution and mineralization during the CO_2-contained IWG-brine-shale reaction at various CO_2 concentrations were illustrated as Fig. 7. Where, dissolved sequestration refers to the sequestration of CO_2

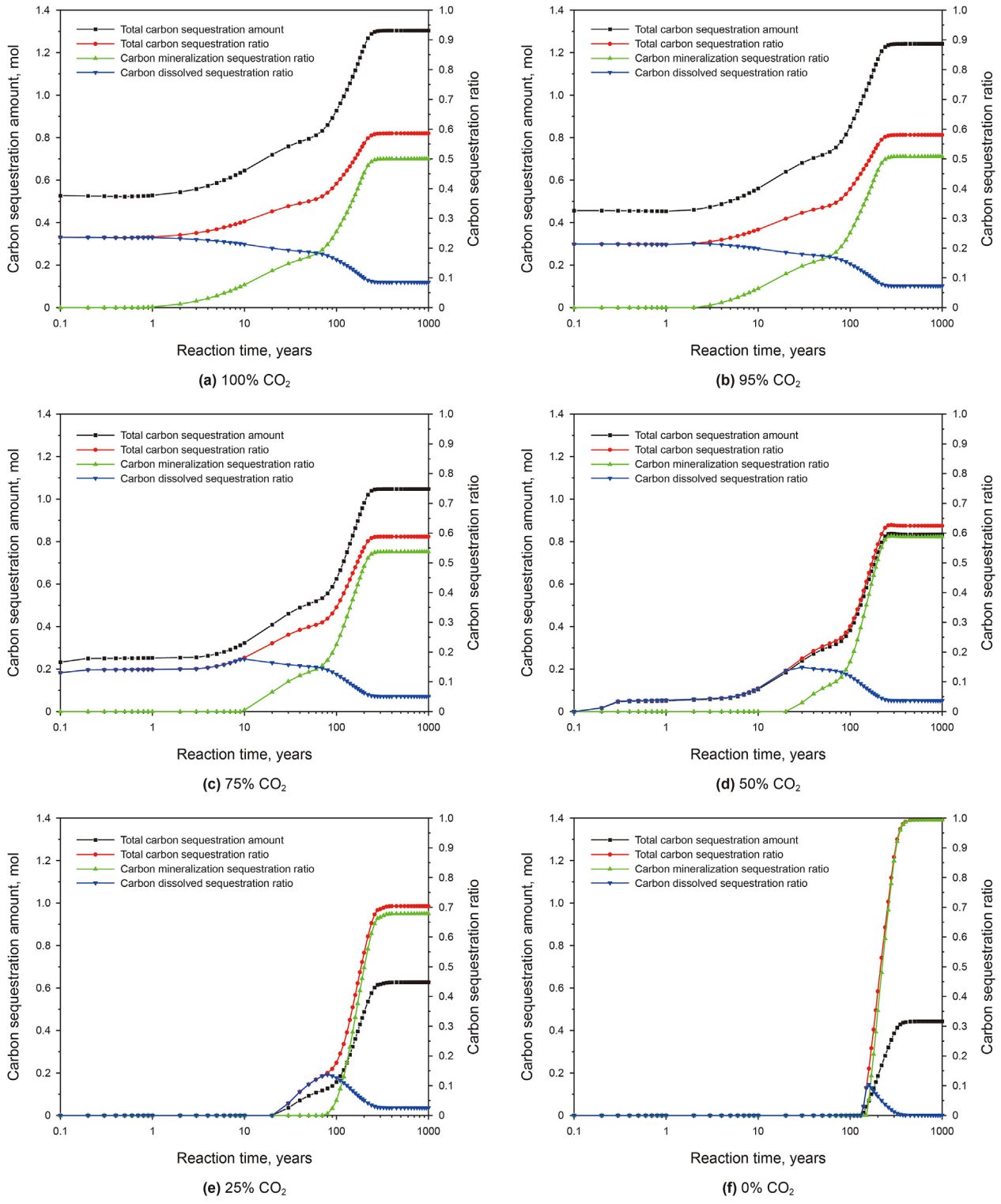

Fig. 7. Changes of sequestration capacity and rate during water-rock reaction with different CO_2 concentrations.

by dissolving it in formation water; mineralization sequestration refers to the generation of bicarbonate and hydrogen ions after CO_2 is dissolved in formation water, which increases the acidity of formation water, thus causing the dissolution of some formation minerals, and further leading to the combination of metal cations and CO_2 in formation water to form some secondary stabilized carbonate minerals, which leads to the sequestration of CO_2 in the formation. So from the results, it can be seen that as initial concentrations of CO_2 from CO_2-contained IWG decreases, the total CO_2 sequestration in the shale reservoir diminishes, while the overall sequestration rate increases. Within the sequestration mechanisms, mineral trapping shows an increase in the sequestration capacity, whereas solubility trapping decreases. In the early stages for the interaction between CO_2-contained IWG, brine, and shale

minerals, the primary mechanism for CO_2 geological sequestration is solubility trapping. As the reaction progresses, at approximately 10 years into the reaction, the precipitation reactions of minerals gradually intensify, resulting in a gradual increase in mineral trapping capacity (Hui et al., 2019; Zhu et al., 2019; Fatah et al., 2022). The trend continues until approximately 300 years into the reaction when it stabilizes. At this point, mineral trapping dominates the CO_2 geological sequestration mechanism, contributing to approximately 90% of the total CO_2 geological sequestration capacity, in line with the simulated results of mineral dissolution/precipitation mentioned earlier. According to numerous studies, mineralization sequestration is the most stable form of geological sequestration of CO_2, and therefore changes in reservoir conditions or fluid chemistry will not destabilize it.

3.2. Water-rock reaction results under different dominant gas

The chemical reactions between CO_2-contained IWG-brine-shale, with different dominant gases, were studied using a kinetic model. The initial concentration of the dominant gas was 50%, with an initial fugacity of 35.0 MPa, while the other gases had an initial concentration of 10% each, with an initial fugacity of 7.0 MPa. The simulation results provided insights into the variations in solution pH, gas solubility, shale mineral dissolution/precipitation, and porosity throughout the CO_2-contained IWG-water-shale reaction.

3.2.1. Changes in pH of aqueous solutions

The changes of solution pH during the CO_2-contained IWG-water-shale reaction at different dominant gases are illustrated in Fig. 8. The results show that after injecting the CO_2-contained IWG with varying dominant gases into the water-shale system for 0.1 year, the pH of the solution decreases from 7.0 to below 4.1 for all cases and gradually increases over the course of 1000 years (Mohd Amin et al., 2014). In the initial stages of the water-rock reaction, the pH of the solutions differs, with the order being SO_2, H_2S, CO_2, HF, NO_2, and CO from lowest to highest. At equilibrium, the pH order is SO_2, CO_2, NO_2, H_2S, HF, and CO from lowest to highest. This pH variation is primarily controlled by the solubility of CO_2 and the different acids produced due to the varying strength of the dominant gases in water. Although CO is sparingly soluble in water, it can undergo redox reactions and converts to CO_2 and dissolve in water, producing the weak acid carbonic acid. On the other hand, while NO_2 is highly soluble in water and forms strong nitric acid, it undergoes intense dissolution reactions with calcite in the initial stages of the reaction, leading to a decrease in pH.

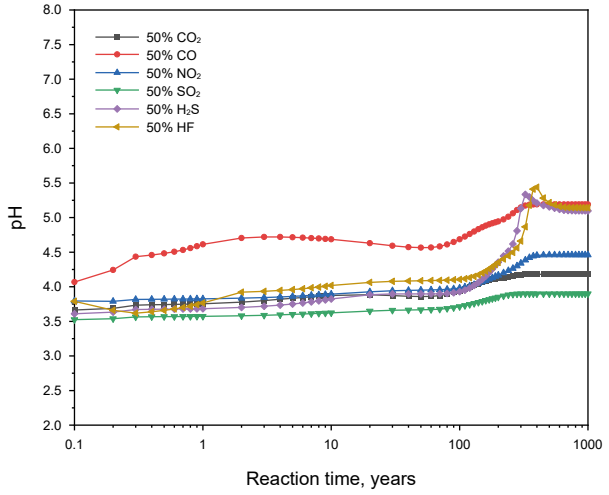

Fig. 8. Changes of pH during water-rock reaction under different dominant gas.

3.2.2. Changes in gas components in the gas phase

The changes of gas components during the CO_2-contained IWG-brine-shale reaction at different dominant gases are illustrated in Fig. 9. The results reveal that after injecting the CO_2-contained IWG with varying dominant gases into the water-shale system for 0.1 year, CO, NO_2, SO_2, and HF are all completely consumed, while H_2S is completely consumed under the NO_2-dominant condition and partially consumed under other dominant gases, and CO_2 in the gas phase not only does not decrease but increases. This phenomenon is due to CO undergoing oxidation reactions and transforming into CO_2, while other IWGs dissolve in water, generating acidic substances. In the initial stages of the reaction, they dissolve calcite, producing a substantial amount of carbonate and bicarbonate ions, leading to the generation of CO_2. As the reaction progresses under different dominant gas conditions, CO, NO_2, SO_2, and HF are consistently entirely consumed in the gas phase. The amount of H_2S in the gas phase is mostly depleted in the initial stages of the reaction, after which it remains nearly constant. However, the concentration of CO_2 in the gas phase increases initially and then gradually decreases over the course of the water-rock reaction, eventually stabilizing after 500 years. The decrease in CO_2 concentration is also as a result of the reduced hydrogen ions concentration in water solution due to shale mineral dissolution/precipitation and, the precipitation of carbonate minerals consumes a substantial amount of carbonate ions in the water solution, leading to significant CO_2 dissolution in water. Additionally, the simulation results indicate that during the process of injecting CO_2-contained IWG for geological sequestration in shale reservoirs, H_2S has a relatively poor solubility in formation water. As water-rock reactions continue, the solubility of H_2S does not significantly increase. This observation suggests that the formation of many sour gas reservoirs may be attributed to such factors (Li and Duan, 2007). Therefore, it is advisable to avoid excessively high H_2S concentrations during the injection of CO_2-contained IWG.

3.2.3. Changes in mineral dissolution/precipitation

The changes of shale porosity during the CO_2-contained IWG-water-shale reaction at different dominant gases are illustrated in Fig. 10. From the simulation results, it is evident that due to the conversion of CO mainly via oxidation reactions into CO_2, the trends in shale mineral changes under CO-dominant conditions closely approximate the results of the CO_2-contained IWG-brine-shale reactions. Under CO-dominant conditions, albite, illite, and montmorillonite completely dissolve; calcite partially dissolves; pyrite hardly participates in the reaction; quartz, K-feldspar, dolomite and secondary minerals like kaolinite and dawsonite, precipitate. As for NO_2 and SO_2, they are highly soluble in water, forming strong acids, and thus, under NO_2 and SO_2 dominant conditions, the trends in shale mineral changes closely resemble the results of the CO_2-contained IWG-water-shale reactions. The mineral transformation trends are similar in both cases, albeit with a higher degree of dissolution/precipitation reactions. Due to the dominance of NO_2 and SO_2, insufficient carbonate ions in the aqueous solution lead to decreased dolomite precipitation, and dawsonite precipitates initially and then gradually dissolves. Furthermore, since nitric acid generated by NO_2 dissolution can dissolve pyrite (Sturmer et al., 2020), it results in partial pyrite dissolution in the presence of higher NO_2 levels in the CO_2-contained IWG, which is not observed in other gas-dominant conditions. Lastly, the results of reactions under H_2S and HF-dominant gases are relatively similar to each other but distinct from reactions under other gases. In comparison to the results of the CO_2-contained IWG-brine-shale reactions,

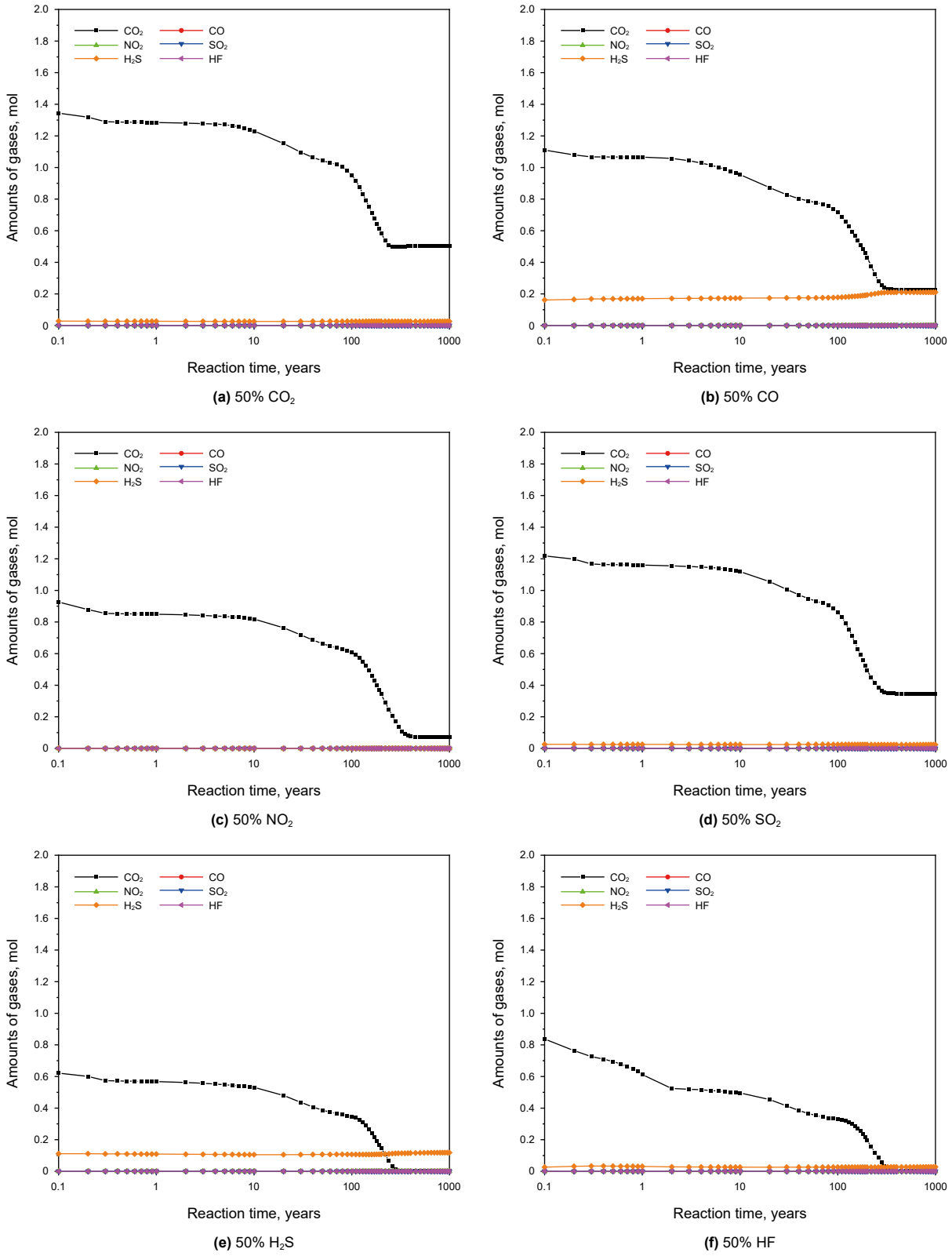

Fig. 9. Changes of gas components during water-rock reaction under different dominant gas.

reactions under H_2S and HF dominant gases also exhibit the dissolution of quartz and the formation of montmorillonite. Additionally, aside from the dawsonite initially precipitating and then entirely dissolving over time, the time to reach equilibrium in water-rock reactions is relatively longer under these two gas-dominant conditions, occurring after about 700 years, which is later than for other gases.

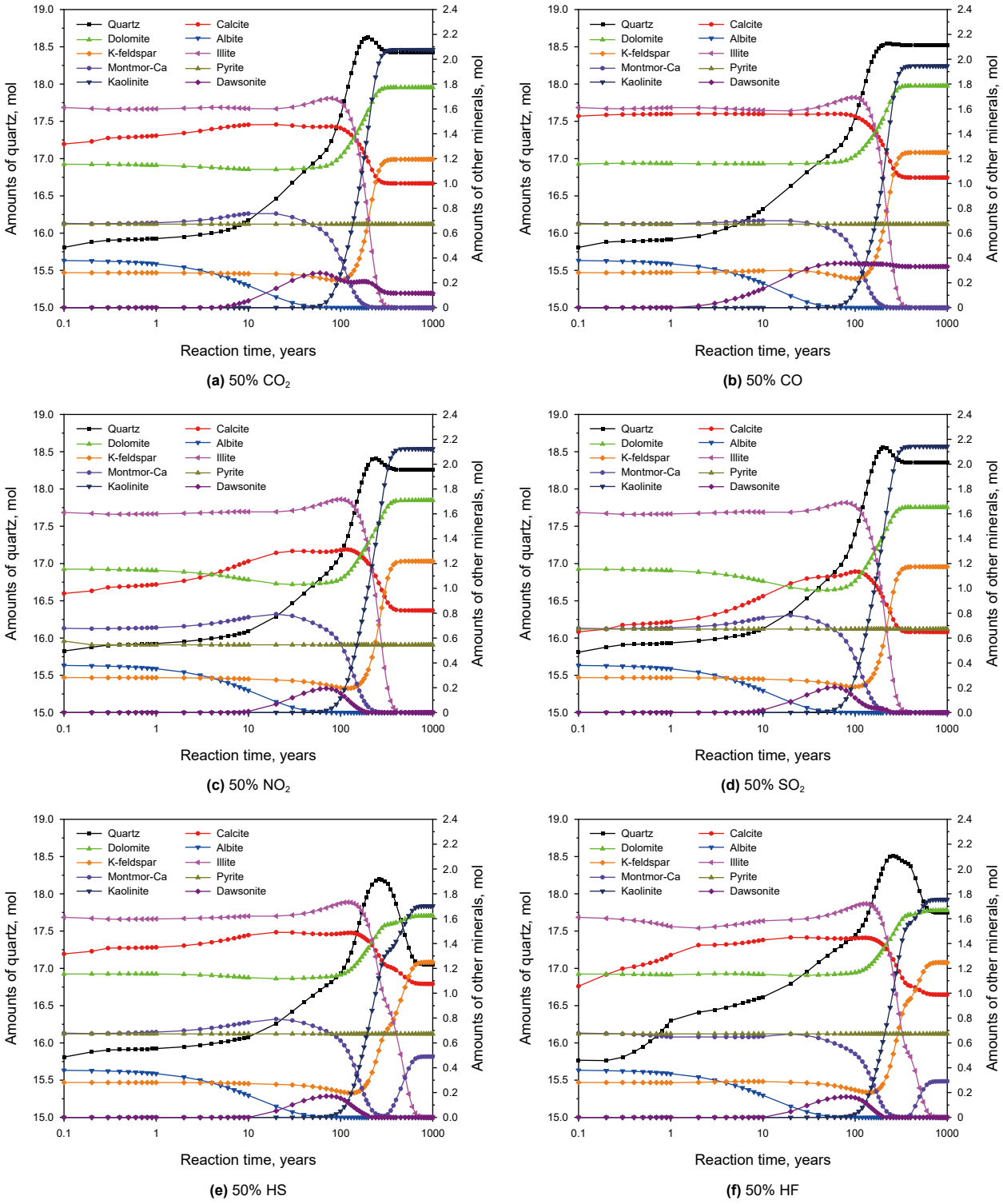

Fig. 10. Changes of shale minerals during water-rock reaction under different dominant gas.

3.2.4. Changes in shale porosity

The changes of shale porosity during the CO_2-contained IWG-water-shale reaction at different dominant gases are illustrated in Fig. 11. According to the results, after injecting CO_2-contained IWG dominated by different gases into the water-shale system for 0.1 year, the porosity of the rock increases, and subsequently decreases gradually until reaching stability. Ultimately, the rock porosity is lower than the initial value, which is favorable for the long-term geological sequestration of CO_2-contained IWG in shale formations. Throughout the entire water-rock reaction process, the rock porosity under different dominant gases follows the order from low to high as SO_2, NO_2, HF, H_2S, CO_2, and CO. This is primarily determined by the acidity of the aqueous solution, which can be inferred from the pH of the aqueous solution (Koukouzas et al., 2018; Liu

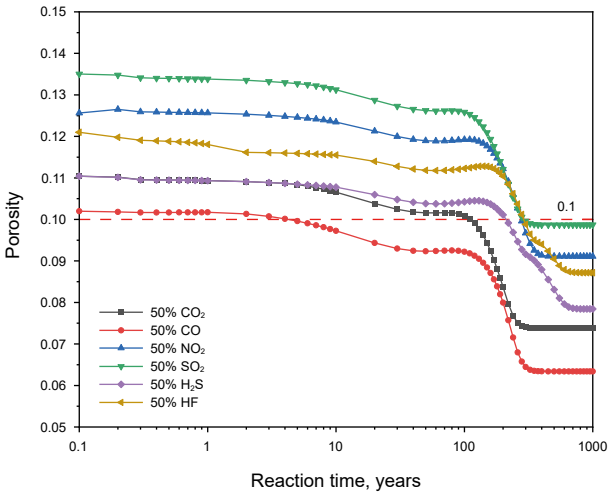

Fig. 11. Changes of shale porosity during water-rock reaction under different dominant gas.

et al., 2019; Zhu et al., 2019). Strong acidity in the aqueous solution promotes the dissolution reactions of shale minerals, resulting in an increase in rock porosity. In contrast, the pH of the aqueous solution under CO_2-dominant conditions, although relatively low, leads to the release of a significant amount of carbonate and bicarbonate ions upon dissolution in water, causing substantial precipitation of carbonate minerals (dolomite and dawsonite). As a result, the rock porosity is lower under these conditions. Additionally, the simulation results suggest that in the early stages of geological sequestration in shale formations under high SO_2 or NO_2 concentrations, the rock porosity significantly increases. This increase is not conducive to the stability of the geological sequestration of CO_2-contained IWG.

The comparative analysis of the chemical reaction results between CO_2-contained IWG dominated by different gases in water-shale mineral systems reveals that when SO_2 is the dominant gas, the water-rock reaction in shale minerals exhibits a more pronounced reactivity. Higher SO_2 concentrations in CO_2-contained IWG result in increased dissolution/precipitation of minerals and have a significant impact on the porosity of shale rocks. According to the simulation results of this model, when the concentration of SO_2 in CO_2-contained IWG exceeds 50%, the porosity of the shale increases significantly and the integrity may be affected. This indicates that in the context of CO_2-contained IWG, SO_2 exerts the most substantial influence on water-rock reactions.

4. Conclusion

This paper established a one-dimensional water-rock chemical reaction kinetic model at the core scale. The model was verified using experimental data and used to simulate the interaction between CO_2-contained IWG and shale. The study revealed the reaction processes among CO_2-contained IWG, water, and shale minerals. It also explored the laws of water-rock reactions under different CO_2 concentrations and dominant gases. The research achieved the following innovative findings.

(1) At equilibrium in the CO_2-contained IWG-water-shale reaction, SO_2, NO_2, HF, and CO are completely consumed. CO_2 is depleted by 56.07% of its initial amount, while H_2S is depleted by 78.94% of its initial amount. Ultimately, 75.71% of the total gas volume is consumed. In terms of shale minerals, albite, illite, and montmorillonite completely dissolve, while calcite partially dissolves. Pyrite barely participates in the reaction, while quartz, K-feldspar, and secondary minerals like kaolinite and dawsonite precipitate. Consequently, the overall mineral content increases by 15.40% compared to the initial amount.

(2) The CO_2-contained IWG-water-shale reaction can be divided into three stages. In the first 10 years, solubility trapping dominates, with only a small amount of mineral dissolution. The porosity of the rocks slightly increases during this stage, posing a risk of gas leakage. During the second stage (10–300 years), mineral dissolution/precipitation reactions intensify. Mineral trapping becomes predominant, and porosity significantly decreases by a minimum of about 40%. After 300 years, the porosity stabilizes around this level. Lower porosity is favorable for long-term geological sequestration of CO_2-contained IWG.

(3) As the initial CO_2 concentration in the CO_2-contained IWG decreases, the initial pH of the solution also decreases from 4.42 to 3.61. This increased acidity enhances mineral dissolution reactions. During the initial stage of the reaction, rock porosity increases by approximately 20%, which affects the stability of geological sequestration. Lower initial CO_2 concentrations lead to a lower total CO_2 sequestration capacity in the CO_2-contained IWG geological sequestration, decreasing from 1.30 to 0.44 mol. However, the total sequestration rate increases from 58.97% to 99.46%. Moreover, the total sequestration rate of CO_2-contained IWG also rises from 58.57% to 98.56%.

(4) H_2S demonstrates relatively poor solubility during the reaction and consumes approximately 80% of its initial amount. Therefore, caution should be exercised when H_2S levels are high during the geological sequestration of CO_2-contained IWG. Additionally, when the content of SO_2 and NO_2 in CO_2-contained IWG reaches 50%, mineral dissolution in the initial stages of water-rock reactions significantly increases. The porosity of the rocks increases by 35.04% and 26.52%, respectively. Therefore, during the geological sequestration of CO_2-contained IWG, there should be consideration for the risk of gas leakage when SO_2 or NO_2 levels are high.

(5) In the early stages of geological sequestration of CO_2-contained IWG in shale reservoirs, increased porosity allows gases to diffuse into a wider range, thereby increasing gas sequestration capacity. As water-rock reactions progress, porosity gradually decreases, preventing gas migration and enhancing the stability of geological sequestration. Throughout the entire lifecycle of CO_2-contained IWG geological sequestration, the porosity of the shale significantly decreases, further improving the stability of the sequestration process.

CRediT authorship contribution statement

Yi-Fan Wang: Writing – original draft, Software, Formal analysis, Data curation. **Jing Wang:** Writing – review & editing, Project administration, Methodology, Investigation, Conceptualization. **Hui-Qing Liu:** Validation, Resources, Funding acquisition. **Xiao-Cong Lv:** Visualization. **Ze-Min Ji:** Supervision.

Conflict of interest

The authors declare that they have no known competing financial interests or personal relationships that could have appeared to influence the work reported in this paper.

Acknowledgements

The work was supported by the National Natural Science Foundation of China (No. 52074316) and PetroChina Company Limited (grant number 2019E-2608).

References

Ao, X., Lu, Y., Tang, J., et al., 2017. Investigation on the physics structure and chemical properties of the shale treated by supercritical CO_2. J. CO_2 Util. 20, 274–281. https://doi.org/10.1016/j.jcou.2017.05.028.

Bhuiyan, M.H., Agofack, N., Gawel, K.M., et al., 2020. Micro- and macroscale consequences of interactions between CO_2 and shale rocks. Energies 13 (5), 1167. https://doi.org/10.3390/en13051167.

Cheng, Y., Zeng, M., Lu, Z., et al., 2020. Effects of supercritical CO_2 treatment temperatures on mineral composition, pore structure and functional groups of shale: Implications for CO_2 sequestration. Sustainability 12 (9), 3927. https://doi.org/10.3390/su12093927.

Chialvo, A.A., Vlcek, L., Cole, D.R., 2013. Acid gases in CO_2-rich subsurface geologic environments. Rev. Mineral. Geochem. 77 (1), 361–398. https://doi.org/10.2138/rmg.2013.77.10.

Crandell, L.E., Ellis, B.R., Peters, C.A., 2010. Dissolution potential of SO_2 Co-injected with CO_2 in geologic sequestration. Environmental Science & Technology 44 (1), 349. https://doi.org/10.1021/es902612m.

De Silva, G.P.D., Ranjith, P.G., Perera, M.S.A., 2015. Geochemical aspects of CO_2 sequestration in deep saline aquifers: a review. Fuel 155, 128–143. https://doi.org/10.1016/j.fuel.2015.03.045.

Ellis, B.R., Crandell, L.E., Peters, C.A., 2010. Limitations for brine acidification due to SO_2 co-injection in geologic carbon sequestration. Int. J. Greenh. Gas Control 4 (3), 575–582. https://doi.org/10.1016/j.ijggc.2009.11.006.

Fatah, A., Bennour, Z., Ben, M.H., et al., 2020. A review on the influence of CO_2/shale interaction on shale properties: Implications of CCS in shales. Energies 13 (12), 3200. https://doi.org/10.3390/en13123200.

Fatah, A., Mahmud, H., Bennour, Z., et al., 2021. Effect of supercritical CO_2 treatment on physical properties and functional groups of shales. Fuel 303, 121310. https://doi.org/10.1016/j.fuel.2021.121310.

Fatah, A., Mahmud, H.B., Bennour, Z., et al., 2022. The impact of supercritical CO_2 on the pore structure and storage capacity of shales. J. Nat. Gas Sci. Eng. 98, 104394. https://doi.org/10.1016/j.jngse.2021.104394.

Fatah, A., Norrman, K., Al-Yaseri, A., 2024. Surface chemistry and chemical structure of shale caprocks exposed to CO_2: Implication for sealing integrity. Energy & Fuels 38 (5), 4390–4400. https://doi.org/10.1021/acs.energyfuels.3c04971.

Gaus, I., Azaroual, M., Czernichowski-Lauriol, I., 2005. Reactive transport modelling of the impact of CO_2 injection on the clayey cap rock at Sleipner (North Sea). Chem. Geol. 217 (3–4), 319–337. https://doi.org/10.1016/j.chemgeo.2004.12.016.

Ghayur, A., Verheyen, T.V., Meuleman, E., 2019. Biological and chemical treatment technologies for waste amines from CO_2 capture plants. J. Environ. Manag. 241, 514–524. https://doi.org/10.1016/j.jenvman.2018.07.033.

Gherardi, F., Xu, T., Pruess, K., 2007. Numerical modeling of self-limiting and self-enhancing caprock alteration induced by CO_2 storage in a depleted gas reservoir. Chem. Geol. 244 (1–2), 103–129. https://doi.org/10.1016/j.chemgeo.2007.06.009.

Godec, M., Koperna, G., Petrusak, R., et al., 2013. Potential for enhanced gas recovery and CO_2 storage in the Marcellus Shale in the Eastern United States. Int. J. Coal Geol. 118, 95–104. https://doi.org/10.1016/j.coal.2013.05.007.

Hadian, P., Rezaee, R., 2019. The effect of supercritical CO_2 on shaly caprocks. Energies 13 (1), 149. https://doi.org/10.3390/en13010149.

Hellevang, H., Pham, V.T.H., Aagaard, P., 2013. Kinetic modelling of CO_2-water-rock interactions. Int. J. Greenh. Gas Control 15, 3–15. https://doi.org/10.1016/j.ijggc.2013.01.027.

Huang, L., Ning, Z., Wang, Q., et al., 2019. Kerogen deformation upon CO_2/CH_4 competitive sorption: Implications for CO_2 sequestration and enhanced CH_4 recovery. J. Petrol. Sci. Eng. 183, 106460. https://doi.org/10.1016/j.petrol.2019.106460.

Hui, D., Pan, Y., Luo, P., et al., 2019. Effect of supercritical CO_2 exposure on the high-pressure CO_2 adsorption performance of shales. Fuel 247, 57–66. https://doi.org/10.1016/j.fuel.2019.03.013.

Kang, S.M., Fathi, E., Ambrose, R.J., et al., 2011. Carbon dioxide storage capacity of organic-rich shales. SPE J. 16 (4), 842–855. https://doi.org/10.2118/134583-PA.

Koukouzas, N., Kypritidou, G., Purser, G., et al., 2018. Assessment of the impact of CO_2 storage in sandstone formations by experimental studies and geochemical modeling: the case of the Mesohellenic Trough, NW Greece. Int. J. Greenh. Gas Control 71, 116–132. https://doi.org/10.1016/j.ijggc.2018.01.016.

Kutchko, B.G., Strazisar, B.R., Dzombak, D.A., et al., 2007. Degradation of well cement by CO_2 under geologic sequestration conditions. Environmental Science & Technology 41 (13), 4787–4792. https://doi.org/10.1021/es062828c.

Lasaga, A.C., 1984. Chemical kinetics of water–rock interactions. J. Geophys. Res. 89, 4009–4025. https://doi.org/10.1029/jb089ib06p04009.

Li, D., Duan, Z., 2007. The speciation equilibrium coupling with phase equilibrium in the H_2O-CO_2-NaCl system from 0 to 250 °C, from 0 to 1000 bar, and from 0 to 5 molality of NaCl. Chem. Geol. 244 (3–4), 730–751. https://doi.org/10.1016/j.chemgeo.2007.07.023.

Li, X., Wang, A., Yu, W., 2010. A trend analysis of carbon dioxide emissions based on the energy Demand. Acta Geosci. Sin. 31 (5), 741–748. https://doi.org/10.3975/cagsb.2010.05.19.

Liu, D., Li, Y., Agarwal, R.K., 2016. Numerical simulation of long-term storage of CO_2 in Yanchang shale reservoir of the Ordos basin in China. Chem. Geol. 440, 288–305. https://doi.org/10.1016/j.chemgeo.2016.08.002.

Liu, B., Zhao, F., Xu, J., et al., 2019. Experimental investigation and numerical simulation of CO_2-brine-rock interactions during CO_2 sequestration in a deep saline Aquifer. Sustainability 11 (2), 1–17. https://doi.org/10.3390/su11020317.

Lyu, Q., Long, X., Ranjith, P.G., et al., 2018. Experimental investigation on the mechanical properties of a low-clay shale with different adsorption times in sub-/super-critical CO_2. Energy 147, 1288–1298. https://doi.org/10.1016/j.energy.2018.01.084.

Merey, S., Sinayuc, C., 2016. Analysis of carbon dioxide sequestration in shale gas reservoirs by using experimental adsorption data and adsorption models. J. Nat. Gas Sci. Eng. 36, 1087–1105. https://doi.org/10.1016/j.jngse.2016.02.052.

Middleton, R.S., Carey, J.W., Currier, R.P., et al., 2015. Shale gas and non-aqueous fracturing fluids: Opportunities and challenges for supercritical CO_2. Appl. Energy 147, 500–509. https://doi.org/10.1016/j.apenergy.2015.03.023.

Mohd Amin, S., Weiss, D.J., Blunt, M.J., 2014. Reactive transport modelling of geologic CO_2 sequestration in saline aquifers: the influence of pure CO_2 and of mixtures of CO_2 with CH_4 on the sealing capacity of cap rock at 37 °C and 100 bar. Chem. Geol. 367, 39–50. https://doi.org/10.1016/j.chemgeo.2014.01.002.

Palandri, J.L., Kharaka, Y.K., 2004. A Compilation of Rate Parameters of Water–Mineral Interaction Kinetics for Application to Geochemical Modeling. U.S. Geological Survey Open File Report. https://doi.org/10.3133/ofr20041068.

Pan, Y., Hui, D., Luo, P., et al., 2018. Experimental investigation of the geochemical interactions between supercritical CO_2 and shale: Implications for CO_2 storage in gas-bearing shale formations. Energy & Fuels 32 (2), 1963–1978. https://doi.org/10.1021/acs.energyfuels.7b03074.

Pearce, J.K., Dawson, G.K.W., Law, A.C.K., et al., 2016. Reactivity of micas and caprock in wet supercritical CO_2 with SO_2 and O_2 at CO_2 storage conditions. Appl. Geochem. 72, 59–76. https://doi.org/10.1016/j.apgeochem.2016.06.010.

Rezaee, R., Saeedi, A., Iglauer, S., et al., 2017. Shale alteration after exposure to supercritical CO_2. Int. J. Greenh. Gas Control 62, 91–96. https://doi.org/10.1016/j.ijggc.2017.04.004.

Rochelle, C.A., Czernichowski-Lauriol, I., Milodowski, A.E., 2004. The impact of chemical reactions on CO_2 storage in geological formations: a brief review. Geological Society London Special Publications 233 (1), 87–106. https://doi.org/10.1144/GSL.SP.2004.233.01.07.

Song, X., Guo, Y., Zhang, J., et al., 2019. Fracturing with carbon dioxide: from microscopic mechanism to reservoir application. Joule 3 (8), 1913–1926. https://doi.org/10.1016/j.joule.2019.05.004.

Song, X., Wang, F., Ma, D., et al., 2023. Progress and prospect of carbon dioxide capture, utilization and storage in CNPC oilfields. Petrol. Explor. Dev. 50 (1), 206–218. https://doi.org/10.11698/PED.20220366.

Steefel, C.I., Lasaga, A.C., 1994. A coupled model for transport of multiple chemical species and kinetic precipitation/dissolution reactions with application to reactive flow in single phase hydrothermal systems. Am. J. Sci. 294 (5), 529–592. https://doi.org/10.2475/ajs.294.5.529.

Sturmer, D.M., Tempel, R.N., Soltanian, M.R., 2020. Geological carbon sequestration: modeling mafic rock carbonation using point-source flue gases. Int. J. Greenh. Gas Control 99, 103106. https://doi.org/10.1016/j.ijggc.2020.103106.

Teng, X., Lu, D., Chiu, Y., 2019. Emission reduction and energy performance improvement with different regional treatment intensity in China. Energies 12 (2), 237. https://doi.org/10.3390/en12020237.

Tian, H., Xu, T., Wang, F., et al., 2014. A numerical study of mineral alteration and self-sealing efficiency of a caprock for CO_2 geological storage. Acta Geotechnica 9 (1), 87–100. https://doi.org/10.1007/s11440-013-0225-8.

Turner, L.G., Dawson, G.K.W., Golding, S.D., et al., 2022. CO_2 and NO_x reactions with CO_2 storage reservoir core: NO_x dissolution products and mineral reactions. Int. J. Greenh. Gas Control 120, 103750. https://doi.org/10.1016/j.ijggc.2022.103750.

Van Pham, T.H., Aagaard, P., Hellevang, H., 2012. On the potential for CO_2 mineral storage in continental flood basalts–PHREEQC batch– and 1D diffusion–reaction simulations. Geochem. Trans. 13 (1), 5. https://doi.org/10.1186/1467-4866-13-5.

Wang, J., Wang, Z., Sun, B., et al., 2019. Optimization design of hydraulic parameters for supercritical CO_2 fracturing in unconventional gas reservoir. Fuel 235, 795–809. https://doi.org/10.1016/j.fuel.2018.08.078.

Wang, J., Bai, H., Wang, S., et al., 2022. Feasibility study on using CO_2-rich industrial waste gas replacement for shale gas exploration based on adsorption characteristics. Chem. Eng. J. 443, 136386. https://doi.org/10.1016/j.cej.2022.136386.

Xu, T., Kharaka, Y.K., Doughty, C., Freifeld, B.M., et al., 2010. Reactive transport modelling to study changes in water chemistry induced by CO_2 injection at the Frio-I Brine Pilot. Chem. Geol. 271 (3–4), 153–164. https://doi.org/10.1016/j.chemgeo.2010.01.006.

Xu, T., Zhu, H., Feng, G., et al., 2019. Numerical simulation of calcite vein formation and its impact on caprock sealing efficiency - case study of a natural CO_2 reservoir. Int. J. Greenh. Gas Control 83, 29–42. https://doi.org/10.1016/j.ijggc.2019.01.021.

Yang, G., Ma, X., Feng, T., et al., 2020. Geochemical modelling of the evolution of caprock sealing capacity at the Shenhua CCS demonstration project. Minerals 10 (11), 1009. https://doi.org/10.3390/min10111009.

Yin, H., Zhou, J., Jiang, Y., et al., 2016. Physical and structural changes in shale

associated with supercritical CO_2 exposure. Fuel 184, 289–303. https://doi.org/10.1016/j.fuel.2016.07.028.

Zhan, J., Yuan, Q., Fogwill, A., et al., 2017. A Systematic Reservoir Simulation Study on Assessing the Feasibility of CO_2 Sequestration in Shale Gas Reservoirs with Potential Enhanced Gas Recovery. Carbon Management Technology Conference, Houston, Texas, USA. https://doi.org/10.7122/484390-MS.

Zhang, J., Liu, J., Dong, L., et al., 2022. CO_2 emissions inventory and its uncertainty analysis of China's industrial parks: a case study of the Maanshan Economic and Technological Development area. Int. J. Environ. Res. Publ. Health 19 (18), 11684. https://doi.org/10.3390/ijerph191811684.

Zhou, J., Hu, N., Xian, X., et al., 2019. Supercritical CO_2 fracking for enhanced shale gas recovery and CO_2 sequestration: results, status and future challenges. Advances in Geo-Energy Research 3 (2), 207–224. https://doi.org/10.26804/ager.2019.02.10.

Zhu, C., Anderson, G.M., 2002. Environmental Applications of Geochemical Modelling. Cambridge University Press, Cambridge, UK. https://doi.org/10.1017/CBO9780511606274.

Zhu, H., Xu, T., Tian, H., et al., 2019. Understanding of long-term CO_2-Brine-Rock geochemical reactions using numerical modeling and natural Analogue study. Geofluids 2019, 1–16. https://doi.org/10.1155/2019/1426061.

Zou, C., Wu, S., Yang, Z., et al., 2023. Progress, challenge and significance of building a carbon industry system in the context of carbon neutrality strategy. Petrol. Explor. Dev. 50 (1), 190–205. https://doi.org/10.11698/PED.20220603.